Thermal infrared radiative transfer within three-dimensional vegetation covers

P Guillevic, Jean-Philippe Gastellu-Etchegorry, J Demarty, L Prevot

JOURNAL OF GEOPHYSICAL RESEARCH, VOL. 108, NO. D8, 4248, doi:10.1029/2002JD002247, 2003

Thermal infrared radiative transfer within three-dimensional vegetation covers

P. Guillevic[1] and J. P. Gastellu-Etchegorry
Centre d'Études Spatiales de la Biosphère, Toulouse, France

J. Demarty and L. Prévot
INRA Avignon - Unité CSE, Domaine Saint Paul, Avignon, France

Received 27 February 2002; revised 1 January 2003; accepted 6 January 2003; published 24 April 2003.

[1] The angular distribution of thermal infrared (TIR) radiation emitted by vegetation covers can vary widely depending on environmental conditions and canopy structure. As an aid in the interpretation of TIR remotely sensed data from vegetated surface with incomplete canopies, we developed a three-dimensional radiative transfer model in the thermal infrared domain. The model simulates the TIR radiative budget and upward spectral radiance of vegetation covers. The model is an extension to the TIR region of the DART (Discrete Anisotropic Radiative Transfer) model developed for the short wave domain. Radiative transfer simulation relies on discrete 3-D scene representations, which include any distribution of trees and ground covers, possibly with topography. Propagation of emitted and scattered radiation is tracked with a ray-tracing approach and the discrete ordinate method. The model was successfully tested against a physically based model for homogeneous canopies, and a partial validation was carried out with directional TIR measurements on a cotton row crop. Model simulations are presented to illustrate the influence of the canopy geometric structure on the directional apparent temperature of hypothetical vegetation covers. *INDEX TERMS:* 1878 Hydrology: Water/energy interactions; 6969 Radio Science: Remote sensing; *KEYWORDS:* Thermal infrared, radiative transfer, vegetation covers, three-dimensional canopies

Citation: Guillevic, P., J. P. Gastellu-Etchegorry, J. Demarty, and L. Prévot, Thermal infrared radiative transfer within three-dimensional vegetation covers, *J. Geophys. Res.*, *108*(D8), 4248, doi:10.1029/2002JD002247, 2003.

1. Introduction

[2] Surface temperature sets the boundary conditions for latent and sensible heat exchanges between the vegetation, the soil surface and the atmosphere. Thermal infrared (TIR) remote sensing provides the radiometric temperature (i.e., temperature measured by a radiometer) of terrestrial surfaces at various scales of space and time. Therefore, many studies were developed to estimate surface sensible heat fluxes [*Jackson et al.*, 1977; *Stewart et al.*, 1993; *Lagouarde et al.*, 1996] and surface latent heat fluxes [*Seguin and Itier*, 1983; *Hatfield et al.*, 1983; *Taconet et al.*, 1986; *Seguin et al.*, 1991; *Courault et al.*, 1996; *Chauki et al.*, 1997; *Norman et al.*, 1997] from surface radiometric temperature. For crop canopies, *Jackson et al.* [1977], *Inoue et al.* [1990] and *Fuchs* [1990] showed that the radiometric temperature allows one to describe the plant water stress and thus the soil moisture state. To improve the estimation of surface heat fluxes, several numerical approaches [*Ottlé and Vidal-Madjar*, 1994; *Taconet et al.*, 1995; *Olioso et al.*, 1999; *Demarty*, 2001] were based on the assimilation of radiometric temperature or soil moisture inferred from infrared observations in a land surface model.

[3] However, the main problem addressed in most previous studies is that the infrared radiometric measurement, called brightness or apparent temperature, cannot be linked in a simple and direct way to surface temperature. Indeed, the infrared radiance represents an integration of radiative fluxes that originate from leaves at different level in the canopy, soil and atmosphere, all of which being usually at different temperatures. Therefore, the apparent temperature depends on various factors [*Fuchs et al.*, 1967; *Kimes et al.*, 1980] such as surface characteristics (canopy structure, temperature distribution, and optical properties), atmosphere properties and configurations of observation (viewing direction and sensor properties). In this context, models are interesting tools to investigate this problem because they make it possible to set up relationships between the TIR observations and surface biophysical parameters. Models simulate the radiance measured by a radiometer, provided that the surface, atmosphere and sensor characteristics are known. In the thermal infrared, two major types of models have been developed for environment studies: geometric projection models and radiative transfer models.

[1]Now at Laboratoire Central des Ponts et Chaussées/Division Eau, Bouguenais, France.

0148-0227/03/2002JD002247

[4] Geometric projection models [*Sutherland and Bartholic*, 1977; *Jackson et al.*, 1979; *Kimes and Kirchner*, 1983a; *Norman and Welles*, 1983; *Sobrino and Caselles*, 1990; *Caselles et al.*, 1992] estimate the TIR radiance of a cover with the help of geometric considerations to describe the canopy structure. First, they calculate the proportions of projected surface area of the different surface components (e.g., sunlit and shaded areas of the canopy and soil), which are directly observed in a particular view direction. Thus, the TIR radiance at the sensor is a weighting of these proportions by the TIR radiances from the respective scene components, which include both contribution of the surface and the atmosphere. Geometric models represent the vegetation as an opaque medium and do not simulate radiative transfer within the cover. Accounting for canopy architecture, geometric models provide a good description of the directional response of TIR sensors. *Jackson et al.* [1977] and *Kimes and Kirchner* [1983a] have validated their model over cotton row crops that were abstracted as parallelepiped solids. However, the major constraint of geometric models is that in order to simulate surface apparent temperature they need the apparent temperature of each scene component, which is generally unavailable and can only be assessed from ground measurements. Moreover, geometric models do not describe the radiative budget within the cover and cannot be coupled easily to land surface models. The latter points limit their use to specific areas where ground radiometric data are available.

[5] Radiative transfer models [*Kimes*, 1980; *Kimes et al.*, 1980; *Smith et al.*, 1981; *Prévot*, 1985; *McGuire et al.*, 1989; *Olioso*, 1995; *François et al.*, 1997; *Olioso et al.*, 1999; *Luquet et al.*, 2001; *Luquet*, 2002] estimate the cover radiance as a function of sensor viewing direction, temperature distribution, and leaf angle distribution within the canopy. They simulate the propagation and the interactions within the cover of TIR radiation emitted by the cover components or incoming from the atmosphere. The canopy is represented as a set of plane elements (i.e., the leaves) statistically distributed into homogeneous horizontal layers. The upward and downward radiative contributions of each layer are based upon the concept of directional gap frequency through the vegetation. The directional radiance of the cover is calculated by summing the radiative contributions of all layers. Iterations are performed to account for multiple scattering within the cover. The first generation radiative transfer models do not account for the canopy three-dimensional architecture. These models were essentially developed and used for homogeneous crops. *Kimes et al.* [1980] and *Prévot* [1985] have validated their model over wheat and corn crops, respectively.

[6] Here, we present a three-dimensional radiative transfer model, the DART (Discrete Anisotropic Radiative Transfer) model, which simulates the TIR radiance of vegetation covers with incomplete canopy. Compared to previous radiative transfer models developed in the thermal infrared, the main originality of the DART model is its ability to take into account the three-dimensional structure of vegetation canopies. After the description of the model, we present tests of this model against a radiative transfer model for homogeneous canopies [*Prévot*, 1985]. We also tested the validity of the model with directional TIR measurements made by *Kimes and Kirchner* [1983a] over a cotton row crop. Finally, we present the sensitivity of the DART model to its major input parameters in order to illustrate the influence of canopy structure on directional brightness temperature in the case of tree covers and row crops.

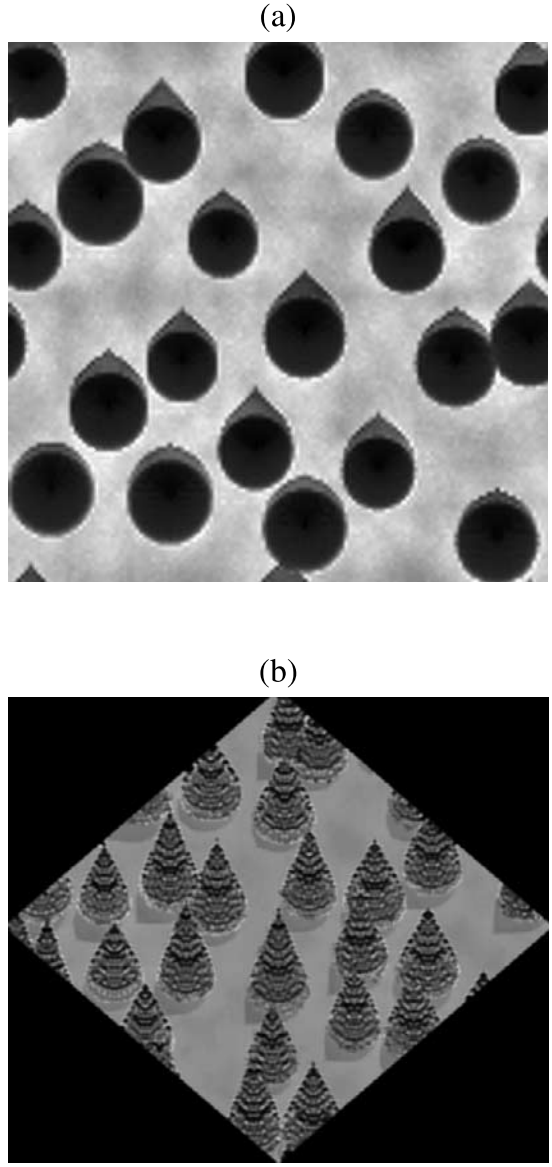

Figure 1. Directional images of a spruce stand. The sun zenith angle is 30°. (a) View in the nadir direction. (b) View in a specific off-nadir direction: viewing zenith angle is 30°; relative azimuth angle is 45°. The spatial resolution is 0.25 m.

2. Model Description

[7] The DART model simulates thermal infrared radiative transfer within heterogeneous vegetation covers characterized by a three-dimensional structure. The model predicts the surface directional radiance and the distribution of thermal energy budget within the canopy over narrow spectral bands or over the entire emission spectrum. It also simulates directional remotely sensed images (Figure 1).

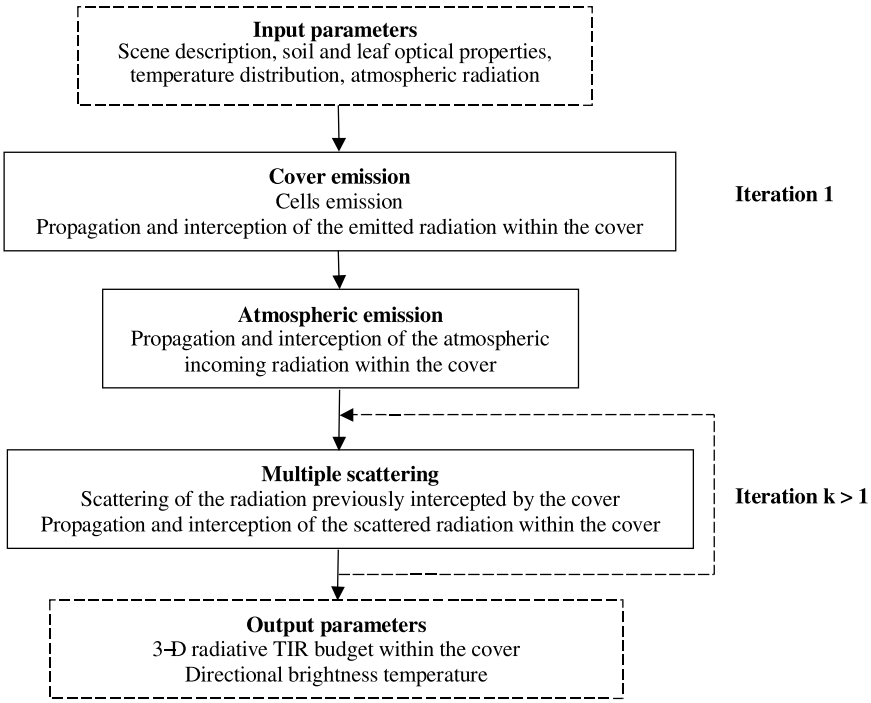

Figure 2. Schematic representation of radiative transfers within the canopy.

Originally, the model was developed for the short wave domain [*Gastellu-Etchegorry et al.*, 1996]. In the visible and near infrared domain, it was validated over three experimental sites (black spruce, jack pine, and aspen) of the BOREAS project [*Gastellu-Etchegorry et al.*, 1999] and over a maritime pine stand located in southeastern France [*Guillevic*, 1999]. We present here its extension to the thermal infrared domain.

[8] As already mentioned, the main originality of the DART model is to take into account the three-dimensional distribution of the scene components characteristics: vegetation density, optical properties and thermodynamic temperatures. Radiative transfer is simulated through three major steps (Figure 2): (1) the scene emission and propagation of the emitted radiation within the cover; (2) the atmospheric emission and propagation of the incoming radiation within the cover; (3) multiple scattering of previously intercepted radiation within the cover. Radiation propagation is tracked with a ray tracing approach combined with the discrete ordinate method. The cover representation, physical processes related to thermal emission and the mathematical approach we adopted to simulate radiative transfer are described in the following subsections.

2.1. Scene Description

[9] The landscape is divided into rectangular cells with variable dimension. Each cell represents one of the cover components such as tree leaves, grass, trunk, soil, and water surfaces (Figure 3). The main parameters required to describe the cover architecture are the tree density, the shape and dimension of the trees, and the topography. Depending on ground data that are available, the scene can be represented with varying degrees of complexity. For example, the position and size of the trees can be specifically prescribed for each tree or statistically defined.

[10] The information content of any cell is specific to that cell and is constant within the cell. Leaf cells (trees and grass) are characterized by their thermodynamic temperature, spectral emissivity, leaf area density, and leaf angle distribution. Soil and trunk cells are described by their thermodynamic temperature and spectral emissivity.

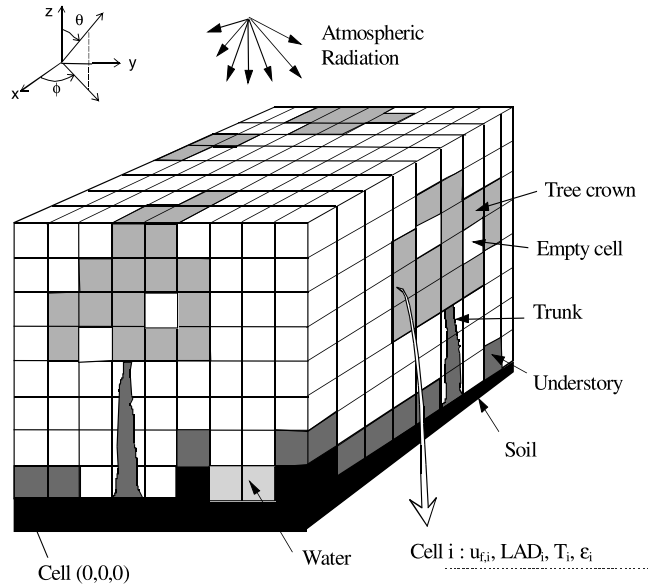

Figure 3. Cell matrix representation of a tree stand. Each cell represents one component of the cover such as leaves, grass, trunks and soil. Leaf cells are characterized by their temperature (T), spectral emissivity (ε), leaf area density u_f ($m^2\ m^{-3}$), and leaf angle distribution (LAD). Soil cells are described by their temperature and spectral emissivity.

[11] Leaves are represented as small plane elements randomly distributed within so-called leaf-cells. From the radiative viewpoint, these leaf cells correspond to turbid media. They give rise to volume interaction processes. Soil is represented by an opaque media and gives rise to surface interaction processes only.

[12] The emissivity of most terrestrial materials depends on wavelength. *Sabins* [1987], *Elvidge* [1988], *Labed and Stoll* [1991], and *Salisbury and d'Aria* [1992] measured the spectral emissivity of a large set of materials. *Salisbury and d'Aria* [1992], for example, showed that the emissivity of most soil and vegetation types varies significantly over the 8–14 μm band. The DART model allows one to simulate radiative transfer over a prescribed spectral domain. The emissivity of each cover component used as input parameter is the average of spectral emissivities over the selected domain.

[13] The temperature distribution depends on the energetic state of each element within the cover, and is determined by both external environmental factors (atmosphere and soil water conditions) and internal plant factors. In its present form, the DART model does not solve the energy and water budget within the cover. This implies that the 3-D distribution of thermodynamic temperatures within the cover must be prescribed. Two alternative ways to specify the temperature distribution can be selected in the model. Each type of cover components (e.g., soil, grass, trees, etc.) can be represented by (1) a constant temperature within the cover or (2) a range of temperatures characterizing the element temperature in sunlit and shaded areas. In the later case, a preliminary simulation in the visible domain allows to assess the sun illumination within the cover. Then a very simplifying hypothesis is used: "the within canopy 3-D temperature is proportional to the intercepted sun radiation." A third option relies on the input of a 3-D temperature distribution that satisfies the energy budget equilibrium. This approach will be presented in a further paper.

2.2. Directions of Propagation

[14] The DART model relies on the discrete ordinate method; that is, radiation can propagate only along a prescribed number N_{dir} of discrete directions. A particular direction Ω_n is characterized by its zenith angle θ_n and azimuth angle φ_n. It is associated with an angular sector $\Delta\Omega_n$ defined by the zenith angle range $\Delta\theta_n$ and the azimuth angle range $\Delta\varphi_n$. The solid angle is then defined as follows:

$$\Delta\Omega_n = \int_{\Delta\varphi_n} \int_{\Delta\theta_n} |d\mu_n|.d\varphi_n \qquad \text{with} \qquad \mu_n = \cos\theta_n. \quad (1)$$

$$\text{We have :} \qquad \sum_{n=1}^{N_{dir}} \Delta\Omega_n = 4\pi. \quad (2)$$

Hereafter, a specific direction Ω_n will be represented by the vector (θ_n, φ_n, $\Delta\Omega_n$).

2.3. Cover Emission

[15] In a first step, the radiative transfer model calculates the emission of each cell of the scene, and the propagation and interception of the emitted radiation within the cover. The emission of a cell depends on the specific optical and structural characteristics of the elements within the cell. Hereafter, we present the approach used to calculate the emission of a soil cell and a leaf cell that are characterized by surface and volume interaction mechanisms, respectively. We assume that for each cell, the origin of any emitted radiation can only be the center of one of the cell sides.

2.3.1. Emission Laws

[16] The Planck's radiation law describes the spectral radiance $L_{B,\lambda}$ emitted by a blackbody (i.e., idealized body that absorbs all of the radiation falling onto it and scatters none) with a temperature T. The emitted radiation is assumed to be isotropic. The Planck's law is:

$$\frac{\partial L_{B,\lambda}(T)}{\partial\lambda} = \frac{2h\lambda^{-5}c^2}{\exp\left(\frac{hc}{\lambda kT}\right) - 1}, \quad (3)$$

where c is the speed of light ($c \sim 2.997925 \times 10^8$ m s^{-1}), h is the Planck's constant ($h \sim 6.62618 \times 10^{-34}$ J s), k is the Boltzmann's constant ($k \sim 1.38066 \times 10^{-23}$ J K^{-1}) and λ is the wavelength.

[17] The total radiance of the blackbody L_B over the emission spectrum, that is, the integration of the Planck's law over the emission spectrum, is given by the Stephan-Boltzmann's radiation law:

$$L_B(T) = \int_0^\infty L_{B,\lambda}(T)d\lambda = \frac{\sigma T^4}{\pi}, \quad (4)$$

where σ is the Stefan-Boltzmann's constant ($\sigma \sim 5.669 \times 10^{-8}$ W m^{-2} K^{-4}).

[18] In the case of natural elements, the spectral radiance L emitted at wavelength λ and the radiance emitted over the entire emission spectrum are given by the equations:

$$L(\lambda, T) = \varepsilon_\lambda.L_{B,\lambda}(T) \quad (5a)$$

$$L(T) = \varepsilon.L_B(T), \quad (5b)$$

where ε_λ and ε are the emissivities of the element for a specific wavelength λ and over the emission spectrum, respectively. $L_{B,\lambda}$ and L_b are given by equations (3) and (4), respectively.

2.3.2. Soil Cells

[19] The origin of the emission of any soil cell is either the center of the topside cell or the center of the cell lateral sides, depending on local topography. For a specific side characterized by a normal vector n_{side} and a temperature T, spectral radiation W_{side} emitted along any direction $\Omega_v(\theta_v, \varphi_v, \Delta\Omega_v)$ is given by:

$$W_{side}(\lambda, T, \Omega_v) = L(\lambda, T).\cos\psi_{nv}.dS.\Delta\Omega_v, \quad (6)$$

where L is the soil spectral radiance given by equation (5a), dS is the area of the cell side and ψ_{nv} is the angle between the normal vector n_{side} and the direction Ω_v.

2.3.3. Trunk Cells

[20] Each trunk is represented within a vertical column of cells (Figure 3). A trunk cell is characterized by a gap fraction

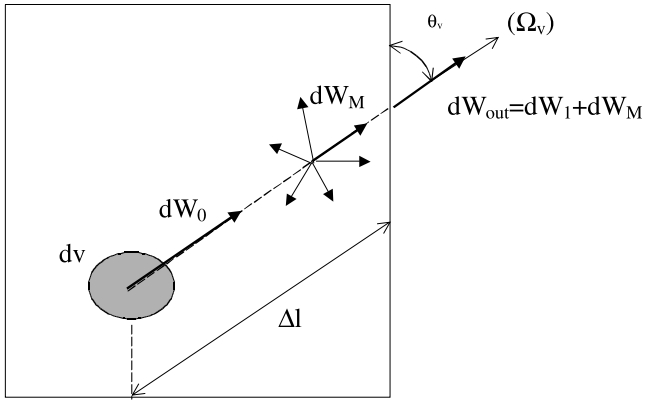

Figure 4. Radiative contribution of a volume dv of leaves to the spectral emission of a leaf cell in a direction Ω_v. The TIR radiation emerging from the cell (dW_{out}) in the direction Ω_v consists of the radiation emitted by the volume dv (dW_0) attenuated through the path Δl (dW_1), and the multiple scattering (dW_M) in the direction Ω_v of the fraction of dW_0 intercepted through the path Δl. All radiative components depend on the volume dv, the temperature of the leaves, the wavelength, and the direction of emission.

(or transmittance of the cell) that depends on the trunk diameter - the exact position of the trunk within a cell is not considered. We assume that the emission of any trunk cell is tracked from the center of its lateral sides. For a specific side, the emitted radiation along any direction Ω_v is given by equation (6) with $dS = dz.Ø_{trunk}$, where dz is the cell height and $Ø_{trunk}$ is the trunk diameter that can vary with height.

2.3.4. Leaf Cells

[21] The radiation W_{cell} emitted by a leaf cell along any direction Ω_v is made of two radiative components: the radiation that is emitted by all leaves without any within cell scattering, and the radiation that is scattered by leaves after being emitted and intercepted by the cell elements (Figure 4). Its expression is:

$$W_{cell}(\lambda, T, \Omega_v, T) = W_1(\lambda, \Omega_v, T) + W_M(\lambda, \Omega_v, T), \quad (7)$$

where W_1 is the first order radiation due to emission processes only and W_M is the scattering contribution. T is the temperature of the cell and λ the wavelength.

[22] Radiation W_{cell} is computed as the integration over the cell volume V_{cell} of the radiative contribution to the cell emission of elementary volume elements dv that make up the cell. The radiation dW_0 emitted by an elementary volume dv along any direction Ω_v is given by:

$$dW_0(\lambda, \Omega_v, T, dv) = L(\lambda, T).d\Sigma(\Omega_v).\Delta\Omega_v \quad (8)$$

with

$$d\Sigma(\Omega_v) = G(\Omega_v).u_f.dv, \quad (9)$$

where $L(\lambda,T)$ is the leaf spectral radiance given by equation (5a), $d\Sigma$ is the apparent cross section of leaves along the direction Ω_v, $G(\Omega_v)$ is the mean projection of a unit foliage area on a surface unit perpendicular to the direction Ω_v, and u_f is the leaf area density.

[23] Radiation dW_0 is then attenuated within the cell along the propagation path Δl (Figure 4). The intercepted fraction dW_{int} of the radiation along paths Δl, for any direction Ω_v, gives rise to the scattering component dW_M along the direction Ω_v. The nonintercepted fraction dW_1 that escapes the cell (Figure 4) is given by:

$$dW_1(\lambda, \Omega_v, T, dv) = dW_0(\lambda, \Omega_v, T, dv).e^{-G(\Omega_v).u_f.\Delta l.} \quad (10)$$

[24] By integration over the cell volume V_{cell}, we have:

$$W_1(\lambda, \Omega_v, T) = \int_{V_{cell}} dW_1(\lambda, \Omega_v, T) \quad (11)$$

$$W_1(\lambda, \Omega_v, T) = L(\lambda, T).G(\Omega_v).u_f.\Delta\Omega_v. \int_{V_{cell}} e^{-G(\Omega_v).u_f\Delta l}.dv. \quad (12)$$

[25] The numerical integration over the cell was performed by discretizing each cell side into a number $I \times J$ of subsides S_{ij} with $i \in [1, I]$ and $j \in [1, J]$ (Figure 5). The volume element dv depends on the emission direction Ω_v considered. We have:

$$dv = S_{ij}.dl.\cos\psi_{nv}, \quad (13)$$

where ψ_{nv} is the angle between a unit vector perpendicular to the subside S_{ij} and the direction Ω_v.

[26] The within cell intercepted radiation W_{int} is the difference between the total radiation emitted by the leaves and the actual radiation that escapes the cell. We have:

$$W_{int}(\lambda, T) = \sum_{v=1}^{N_{dir}} [L(\lambda, T).G(\Omega_v).u_f.V_{cell}.\Delta\Omega_v - W_1(l, \Omega_v, T)], \quad (14)$$

where N_{dir} is the number of discrete directions.

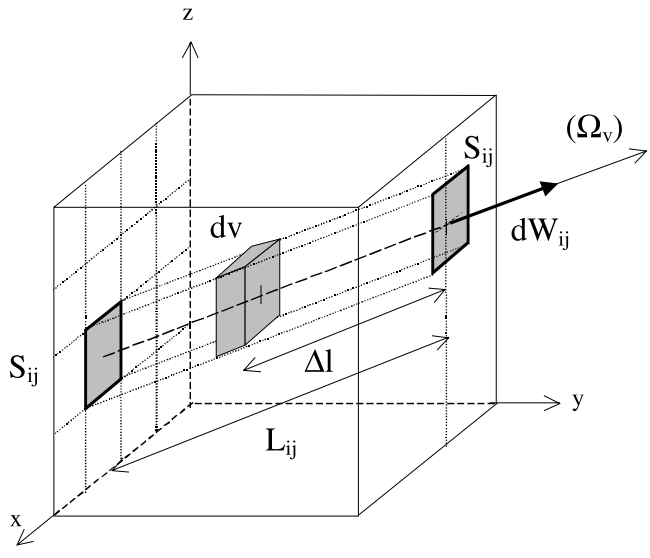

Figure 5. Summation scheme to calculate the emission of a leaf cell. The cell sides are decomposed in $i \times j$ elementary areas S_{ij}. The component dW_{ij} of the total cell radiation in the direction Ω_v is computed by integration along the path L_{ij} of the radiation emitted by a volume dv of leaves. The approach accounts for multiple scattering within the cell.

[27] The intercepted energy gives rise to multiple scattering into the 4π space. Because leaf emissivity is close to unity (i.e., single scattering albedo is close to zero) and because multiple scattering cannot be modeled exactly, we assume that the within cell scattering component is nearly isotropic and originates from the cell's center. These assumptions allow one to define for each leaf cell a mean directional transmittance $\langle T \rangle$ from the center to a side of the cell and a mean single scattering albedo ω_λ. We have:

$$\langle T \rangle = \frac{1}{4\pi} \int_{4\pi} e^{-G(\Omega_v).u_f.\Delta m(\Omega_v)} d\Omega_v \tag{15}$$

$$\omega_\lambda = \frac{1}{4\pi} \int_{4\pi} \int_{4\pi} f(\Omega_i \rightarrow \Omega_v) d\Omega_i d\Omega_v, \tag{16}$$

where $\Delta m(\Omega_v)$ is the path along the direction Ω_v from the center of the cell to the cell side from which the radiation escapes. $f(\Omega_i \rightarrow \Omega_v)$ is the leaf scattering phase function; Ω_i is the incident direction of the radiation and Ω_v is the scattering direction. The phase function also depends on the leaf angle distribution and optical properties. Leaf thermal infrared phase functions are calculated as the leaf phase functions in the short wave domain [*Gastellu-Etchegorry et al.*, 1996].

[28] The total scattered radiation that escapes the cell is then given by the following analytical formulation:

$$W_M(\lambda, T) = W_{int}(\lambda, T).\Big\{\omega_\lambda.\langle T \rangle + \omega_\lambda.\langle T \rangle.[\omega_\lambda - \omega_\lambda.\langle T \rangle] + \omega_\lambda.\langle T \rangle.[\omega_\lambda - \omega_\lambda.\langle T \rangle]^2 + ..\Big\}. \tag{17}$$

We have:

$$W_M(\lambda, T) = \frac{\omega_\lambda \langle T \rangle}{1 - \omega_\lambda(1 - \langle T \rangle)} W_{int}(\lambda, T). \tag{18}$$

[29] The directional distribution of the scattered radiation W_M is assumed to be proportional to the solid angle $\Delta\Omega_v$ and to the apparent leaf cross section along any direction Ω_v [*Gastellu-Etchegorry et al.*, 1996].

2.4. Incoming Atmospheric Radiation

[30] The incoming radiation due to the thermal emission of the atmosphere is assumed to be isotropic. It can be directly prescribed as a model input parameter. Moreover, it can be assessed either with the spectral analytical model of *Berger* [1988], for a limited bandwidth, or with the model of *Brutsaert* [1975] if it is considered the whole spectrum. The two models require the air temperature and the air humidity at 2 meters above the soil.

2.5. Radiation Propagation and Multiple Scattering Within the Cover

[31] As already mentioned, the DART model simulates radiative transfer along a set of discrete directions. During the propagation within the cover, radiative fluxes interact with individual cells. Interaction processes within a cell depend on the nature of the cell (i.e., structural and optical properties). The incoming radiation is transmitted through gaps (e.g., empty cells), totally intercepted by opaque cells (e.g., soil and water cells) or partially attenuated by semiopaque cells (e.g., trunk and leaf cells). The propagation stops when radiative fluxes are totally intercepted by the cover elements or when it escapes from the upper cells of the scene.

[32] Intercepted radiation is computed through calculation of the exact propagation path within the cell. In a further step, this intercepted radiation is scattered. An iterative approach is used to account for multiple scattering within the cover. During any iteration, the model (1) computes the radiation scattered by any cell that intercepted radiation in the previous iteration, and (2) tracks this scattered radiation within the scene. Radiation that escapes from the upper cells of the scene is stored at each iteration, and contributes to the upward radiance of the scene. Actually, simulations tend to converge after two iterations only because most terrestrial materials have a low reflectance in the TIR domain. However, multiple scattering cannot be neglected. The contribution to the cover radiance of radiation that is scattered after being emitted by the cover and subsequently intercepted (i.e., atmospheric radiation is neglected) is represented in Figure 6. The importance of multiple scattering mostly depends on the optical properties of the soil and leaves and on the Leaf Area Index (LAI). The influence of scattering processes on the apparent temperature was assessed with a series of theoretical simulations conducted with variable LAI (from 1 to 6) and leaf emissivity ε_f (from 0.94 for brown leaves to 0.98 for green leaves), and a soil emissivity equal to 0.96. In the nadir viewing direction, multiple scattering increases the apparent temperature by more than 1 K if leaf emissivity is 0.98 and more than 2 K if leaf emissivity is 0.94. The latter case represents nevertheless an extreme value for vegetation emissivity.

3. Model Validation

[33] To verify the approach adopted by the DART model to simulate radiative transfer, we first tested the model against a physically based model [*Prévot*, 1985] adapted to homogeneous canopies. Then, a first validation was carried out with directional radiometric measurements made by *Kimes and Kirchner* [1983a] over a cotton row crop.

3.1. Comparison With the Model of Prévot

[34] We compared the apparent temperatures of homogeneous turbid canopies simulated by the DART model and by the model of *Prévot* [1985]. The latter model was derived from the radiative transfer approach described by *Kimes* [1980]. It simulates radiative transfer within vegetated canopies represented as a set of plane elements (i.e., the leaves) statistically distributed into ten homogeneous horizontal layers. The upward and downward radiative contributions of each layer are based upon the concept of directional gap frequency through the vegetation. The model was validated with radiometric measurements made over corn crops and was used in several studies [*Paw U*, 1992; *François et al.*, 1997]. It is a reference model provided that the canopy can be reliably represented by homogeneous horizontal layers.

[35] The comparison study was feasible because both models specify in a similar way the thermal properties and the geometry (in the case of homogeneous canopies)

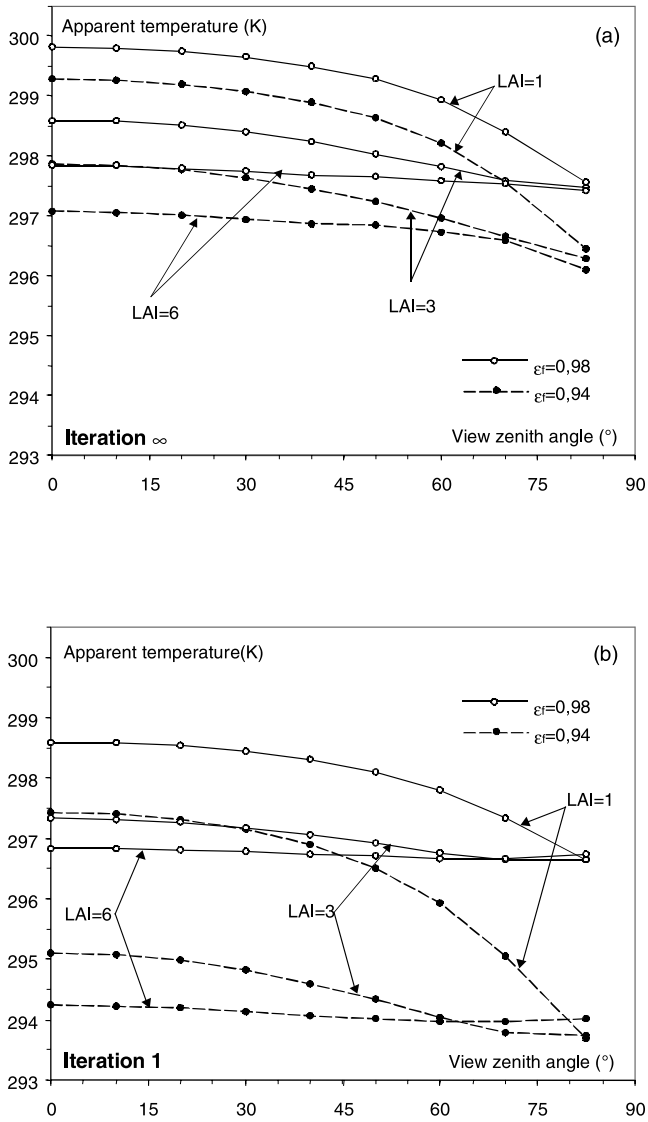

Figure 6. Influence of multiple scattering within the canopy on the directional apparent temperature of a homogeneous cover simulated with the DART model. (a) Cover emission and multiple scattering (Iteration ∞). (b) Cover emission only (Iteration 1). The soil emissivity is 0.96. The leaf emissivity ε_f is 0.94 or 0.98. The LAI varies from 1 to 6. The temperature of the soil and leaves are 303 K and 298 K, respectively.

of the cover. The comparison was conducted with a vegetation cover for which the LAI is 2, and the soil and leaves temperature are 303 K and 298 K, respectively. We considered two experiments. First, the leaf emissivity is prescribed to 1 and the soil emissivity varies from 0.9 to 1. In the second case, the soil emissivity is prescribed to 1 and the leaf emissivity varies from 0.96 to 1 (Figure 7). Generally speaking, the two models give very similar results. When leaf emissivity is equal to the unit (i.e., no foliar scattering), the two models predict nearly equal apparent temperature whatever the viewing direction. These results allow us to verify the validity of the approach used by the DART model to simulate cover emission processes and soil scattering processes. In the second experiment, with a variable leaf emissivity, the two models give slightly different results. Indeed, compared to the model of Prévot, the DART model tends to overestimate the apparent temperature for large viewing zenith angles and to underestimate it for low zenith angles. Differences are due to the fact that the two models use different approaches for simulating foliar scattering. Indeed, the DART model uses hemispherical-directional phase functions for simulating scattering within vegetation canopies, whereas the model of Prévot uses bi-hemispherical phase functions. Thus, the DART model should be slightly more accurate in its representation of multiple scattering.

3.2. Validation Over a Cotton Row Crop

[36] The validity of the DART model was carried out using data collected by *Kimes and Kirchner* [1983a] over a mature cotton row crop. The authors measured the directional apparent temperature of the crop for various sun positions. The spectral band of the sensor was 8–14 μm and five view zenith angles were sampled (0°, 20°, 40°, 60° and 80°) within the plane normal to the rows and with a south-looking orientation (Figure 8a). The geometric structure of the canopy was described with regard to the row's height and width, and the distance between two consecutive rows. Vegetation rows were abstracted as parallelepipeds. In addition, radiometric data were collected on four scene components: sunlit and shade vegetation, and sunlit and shade soil. Whatever the sun position, the difference observed between the sunlit and shade vegetation was lower than 0.5 K. In our experiment, we assume the vegetation temperature constant within the canopy and equal to the observations mean.

[37] However, the DART model requires the thermodynamic temperature distribution within the canopy. This distribution was not measured by *Kimes and Kirchner* [1983a]. Here, it was assessed using the apparent temperature of the cover measured by the authors in the nadir direction. First, we used images of the crop simulated by the

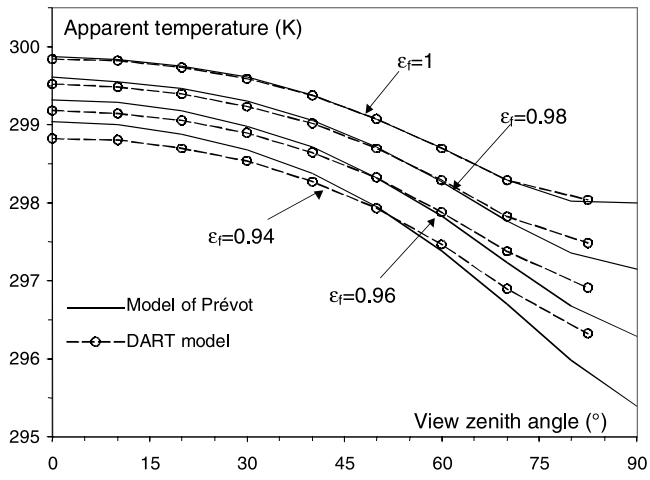

Figure 7. Apparent temperature of a homogeneous cover simulated with the DART model (dotted lines) and the model of *Prévot* [1985] (solid lines). The soil emissivity is 1. The leaf emissivity (ε_f) varies from 0.94 to 1. The LAI is 2. The temperature of the soil and leaves are 303 K and 298 K, respectively.

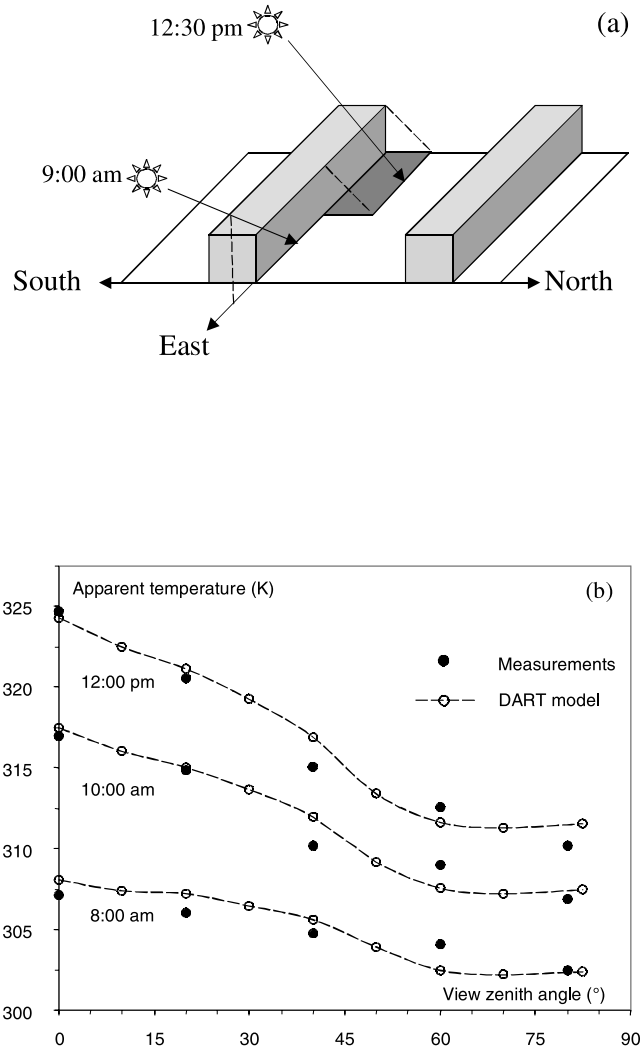

Figure 8. (a) 2-D canopy representation of a cotton row crop. The vegetation rows are abstracted by parallelepipeds. (b) Directional apparent temperature of the crop simulated by the DART model, and measured by *Kimes and Kirchner* [1983a], at three different hours. The viewing direction is in the plane normal to the rows.

DART model to calculate the relative contributions of the canopy, sunlit soil and shade soil to the cover vertical radiance. For each sun position, we then adjusted the thermodynamic temperatures of the canopy, sunlit soil and shade soil to retrieve (1) the apparent temperatures of the three components and (2) the apparent temperature of the cover measured in the nadir. Results are presented in Table 1.

[38] Few other parameters required by the model were not collected by *Kimes and Kirchner* [1983a]. The leaf angle distribution is assumed spherical. The leaf area index is 2.8 according to measurements made by *Huete et al.* [1985] on a mature cotton crop. The soil and leaf emissivities are prescribed to 0.94 and 0.98, respectively. The incoming atmospheric radiation is assumed constant during the day and equal to 350 W m^{-2}.

[39] The predicted sensor responses as a function of view angle versus the radiometric observations are presented in Figure 8b. Results stress the ability of the DART model to simulate the strong anisotropy of the crop thermal radiance. For example, the model predicts the 13 K decrease in the apparent temperature when the view zenith angle varies from 0° to 60° and the sun is at its optimal. This strong temperature decrease is mainly due to two combined factors: the temperature difference between the soil and vegetation, and the canopy geometry. The root mean square (r.m.s.) deviation of the difference between the simulated and measured apparent temperatures for all sun positions and viewing directions is 1.25 K. *Kimes and Kirchner* [1983a] used the thermal observations to validate a geometric projection model specifically designed for row crops. The authors found a r.m.s. deviation of 0.96 with their model. The higher value we obtained with the DART model can be explained by the fact that some parameters required by the model were not collected at ground level. It is not the case for the geometric model that is only driven by the canopy geometry and the apparent temperature of each cover components. However, this first validation test showed that the DART model provides insight to understanding variations in directional sensor response.

4. Factors Affecting the Apparent Temperature of Vegetation Covers

[40] In this section, we evaluate the sensitivity of the DART model to variations in its input parameters that describe the cover (canopy structure, temperature distribution) and its environment (sun position, incoming atmospheric radiation). It should be noted that, although they are analyzed separately, these parameters can be interactive and highly dependent on each other.

4.1. Viewing Direction

[41] Numerous investigations based on ground experiments [*Fuchs et al.*, 1967; *Guyot and Chasseray*, 1981; *Kimes and Kirchner*, 1983a; *Becker et al.*, 1986; *Huband and Monteith*, 1986; *Boissard et al.*, 1990; *Lagouarde et al.*, 1995] or modeling approaches [*Sutherland and Bartholic*, 1977; *Jackson et al.*, 1979; *Kimes et al.*, 1980; *Smith et al.*, 1981; *Kimes and Kirchner*, 1983a; *Prévot*, 1985; *Fuchs*, 1990; *Sobrino and Caselles*, 1990; *François et al.*, 1997] have focused on the influence of the viewing direction on the apparent temperature of vegetation covers. The impact of viewing direction mostly depends on the canopy structure and on the temperature distribution within the cover. Indeed, the directional apparent temperature is directly related to the proportions of various cover components observed by a radiometer. These proportions vary with the viewing direction. When the view zenith angle increases, the soil contribution to cover radiance decreases,

Table 1. Thermodynamic Temperature of the Leaves (T_{leaf}) and Soil in Shade (T_{soil1}) and Sunlit (T_{soil2}) Areas that Allow the DART Model to Retrieve the Apparent Temperatures in the Vertical Direction Measured by Over a Cotton Row Crop (T_{app}) and Its Three Components (Vegetation, Sunlit, and Shade Soil)

	6:00	7:00	8:00	9:00	10:00	11:00	12:00	13:00
T_{app}	299.4	303.3	307.2	313.8	317.0	320.0	324.7	327.8
T_{leaf}	298.0	302.5	303.0	305.3	308.0	310.0	312.0	313.2
T_{soil1}	301.4	302.0	304.5	305.0	309.0	310.5	314.0	317.4
T_{soil2}	301.4	308.3	315.3	320.5	329.0	335.8	340.2	341.3

and the apparent temperature decreases due to the fact that the soil temperature is generally larger than vegetation temperature. The directional variations of the apparent temperature are illustrated in the following sensitivity studies.

4.2. Sun Position and Temperature Distribution

[42] The sun elevation has a major influence on the apparent temperature of a vegetated cover. It defines both the distribution and the amplitude of temperature. The average temperature of each component of the cover increases when sun elevation increases because sun irradiance increases. Temperature distribution within the cover is determined by the penetration of solar radiation within the cover. Consequently, it depends on the sun direction and the canopy structure.

[43] In the case of a cotton row crop, the influence of sun position on temperature distribution, and consequently on the apparent temperature of the canopy, is illustrated in Figure 9. All input parameters used to drive the model were taken from data collected by *Kimes and Kirchner* [1983a]. A description of the data set was given in section 3.2. The architecture of the scene (row orientation) and the relative position of the sun at 9:00 am (the sun direction is parallel to the rows) and 12:30 pm (the sun direction is perpendicular to the rows) are shown on Figure 8a. Figure 9 shows the simulated apparent temperature obtained with a viewing direction within a plane perpendicular to the rows (plane South-North).

[44] Variations of soil and vegetation temperature observed during the day (Table 1) explain why the directional apparent temperature strongly increases when sun elevation increases (i.e., sun zenith angle decreases) (Figure 9). Along the nadir direction, the apparent temperature of the cover varies from 299.5 K at 6 am to 325.7 K at 1 pm.

[45] For a specific sun position (i.e., specific time during the day), Figure 9 illustrates also the strong directional variability of apparent temperature. The apparent temperature is maximal when the viewing zenith angle θ_v is zero (nadir direction) and decreases when θ_v increases because of a decrease of the soil radiative contribution. In the shortwave domain, the cover reflectance is maximal along the "hot spot" direction, that is, the direction for which the target, the radiometer and the sun are lined up. In that case, a radiometer sees sunlit areas only. We could expect that in the thermal infrared domain, the maximal value of the apparent temperature is along the hot spot direction. In the present case, the soil temperature in shaded area is slightly higher than the vegetation temperature during the day, and leaf temperature is assumed to be constant within the cover. Thus, directional variations of the apparent temperature depend only on the proportions of soil (in sunlit and shaded areas) that contributes to the cover radiance, and the apparent temperature is maximum along the nadir direction. However, due to the temperature distribution, the directional distribution of apparent temperature is not symmetric for most sun positions. For a given view zenith angle, the apparent temperature T_{app} is maximal along the direction for which the relative azimuth angle with the sun direction is minimal.

[46] In the plane parallel to the rows (plane East-West), we found that the apparent temperature is quite constant whichever the view zenith angle. Due to the structure of the cover, proportions of the various components seen by a radiometer do not vary with the view zenith angle.

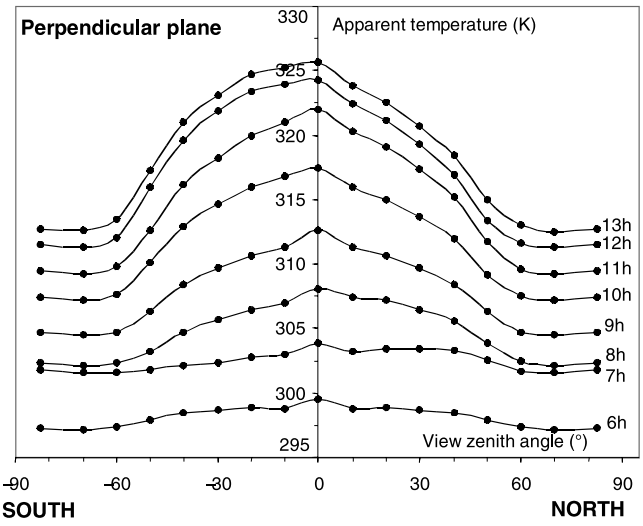

Figure 9. Directional variations in the apparent temperature of a cotton row crop obtained with the DART model for different sun positions. The viewing directions are in the plane normal to the rows.

4.3. Incoming Atmospheric Radiation

[47] The contribution to the apparent temperature of the fraction of the incoming atmospheric radiation reflected by the cover depends on the structural and optical properties of the cover. We evaluated how the thermal atmospheric illumination influences the apparent temperature of two vegetation covers represented with a homogeneous and incomplete canopy, respectively (Figure 10). For that purpose, we made two sets of simulations using the DART model. In the first set, the canopy is represented as a superposition of homogeneous layers. In the second set, the canopy is represented as infinite parallel rows of vegetation covering 50% of the cover (2-D canopy). Except for the representation of the canopy, all parameters describing the cover are similar in both series of simulations. The LAI is 2, the soil and leaf emissivities are 0.94 and 0.98, respectively, and the soil and leaf temperature are 305 K and 298 K, respectively. The incoming atmospheric radiation varies from 0 to 400 W m^{-2}. In the case of vegetation rows, the directional distribution of the apparent temperature is represented in the plane perpendicular to the rows.

[48] For the 2-D representation (Figure 10b), the influence of the incoming atmospheric radiation is higher along directions close to the vertical, for which the soil has a higher contribution to the apparent temperature. However, the impact is low and variations of ±100 W m^{-2} in the atmosphere radiation (R_a) modify the apparent temperature (T_{app}) by about ±0.3 K in the nadir viewing direction. For the homogeneous cover, the impact of the atmosphere is lower and quite constant whichever the viewing direction.

[49] Differences between the two sets of simulations reflect the impact of the canopy structure. These differences are higher for viewing directions close to the nadir for which the soil contribution is lower when the canopy is homogeneous. When the atmosphere contribution is

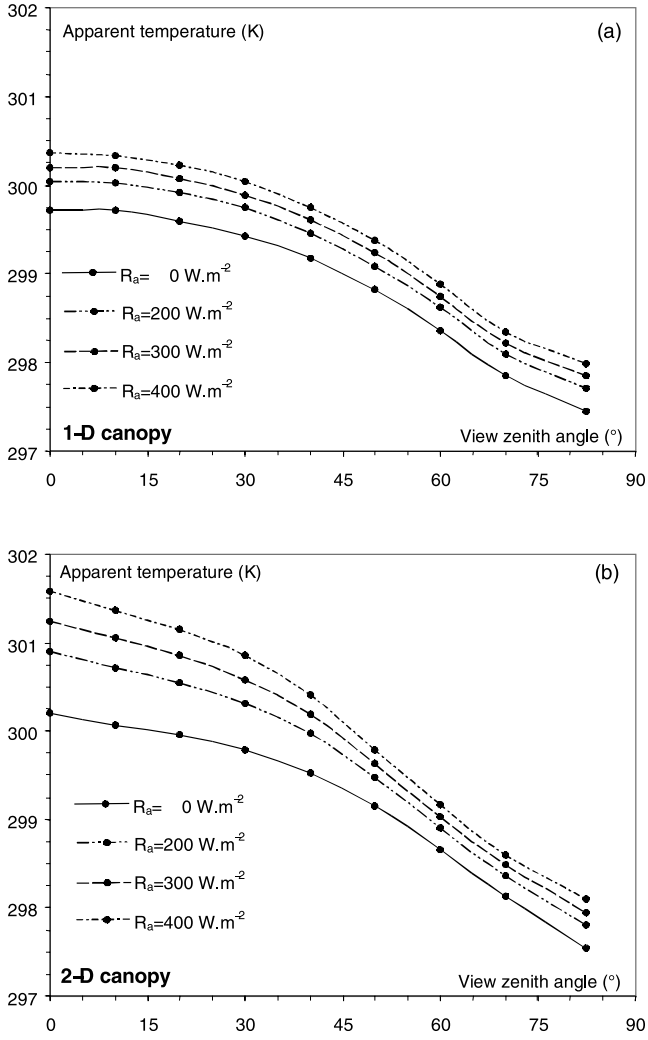

Figure 10. Influence of the incoming atmospheric radiation (R_a) on the apparent temperature of vegetation covers represented with (a) a 1-D canopy and (b) a 2-D canopy. R_a varies from 0 to 400 W m^{-2}. The 1-D canopy is represented by superposed homogeneous layers. The 2-D canopy is represented by vegetation rows (50% ground cover). The LAI is 2. The temperature of the soil and leaves are 305 K and 298 K, respectively.

neglected (case R_a = 0 W m^{-2}), the difference between apparent temperature ΔT_{app} is 0.6 K in the nadir viewing direction. It illustrates the influence of the canopy structure on the cover emission. The difference ΔT_{app} is amplified by the atmospheric contribution and is about 1.2 K when R_a = 400 W m^{-2}. It is negligible for large view zenith angles for which ΔT_{app} is lower than 0.1 K.

4.4. Canopy Structural Parameters

[50] The previous sections stressed the influence of the canopy structure on the directional apparent temperature of vegetation covers. Directional variations of the apparent temperature depend on both the temperature distribution within the cover and the relative contribution of the soil and the vegetation on the directional radiance. The proportions of surface area of soil and canopy that are in direct line of sight in a particular view direction directly depend on the canopy geometric structure. Indeed, *Kimes et al.* [1980] observed very weak directional variations on the apparent temperature of covers characterized by quite homogeneous canopies: (1) a dense and completely senesced canopy (LAI $\sim$ 5.4 and cover fraction is close to 100%) and (2) a very sparse vegetation cover (LAI $\sim$ 0.05). On the other hand, *Kimes and Kirchner* [1983a] measured very strong directional variations of the apparent temperature of a cotton row crop characterized by a strong temperature gradient between the soil and the plants, and a cover fraction around 50% (see section 3.2). The impact of canopy structural parameters (LAI, leaf angle distribution, cover fraction and canopy architecture) is analyzed below.

4.4.1. Leaf Area Index and Canopy Geometry

[51] We evaluated the influence of LAI variations on the apparent temperature of three hypothetical vegetation covers characterized by different canopy geometric structure:

(1) 1-D canopy (Figure 11a). The canopy structure is assumed to be homogeneous and represented by superposed infinite layers of vegetation. The cover fraction is 100%.

(2) 2-D canopy (Figure 11b). The canopy consists of infinite rows of vegetation. The cover fraction is 50%. The row width, the row height, and the distance between two consecutive rows are assumed to be identical and equal to 0.5 m.

(3) 3-D canopy (Figure 11c). The canopy consists of trees randomly distributed over an infinite area. The cover fraction is 50%. The tree crowns are represented by hemi-ellipsoids. The crown's height and width are identical and equal to 2 m. The trunk height is 1.5 m.

[52] For each set of simulations, LAI varies from 1 to 8, the Leaf Angle Distribution (LAD) is spherical, the soil and leaf emissivities are 0.94 and 0.98, respectively, and the soil and leaf temperatures are 298 K and 305 K, respectively.

[53] Whatever the canopy representation, a LAI increase reduces the radiative contribution of the soil on the cover radiance and consequently decreases the directional apparent temperature. However, the directional behavior and the magnitude of apparent temperature variations depend on the canopy geometric structure.

[54] For the 1-D canopy representation (Figure 11a), the influence of LAI variations on the apparent temperature is higher for viewing directions close the nadir direction, and decreases when the view zenith increases. When LAI is 3 and the view zenith angle is 30°, LAI variations ΔLAI of +1 and −1 (i.e., ΔLAI/LAI = ±33%) induce apparent temperature variations of −0.4 K and +0.7 K, respectively. For high LAI, configurations for which the soil contribution is the lowest, the apparent temperature appears more isotropic and converges toward a limit that represents, in first approximation, the combination of the canopy emission and multiple scattering within the canopy. Results obtained for heterogeneous canopies are presented in Figures 11b and 11c. Accounting for the canopy geometry, the soil radiative contribution is higher, and then the directional apparent temperature is higher but globally less sensitive to LAI variations. In comparison to the "1-D canopy" experiment, the impact of a LAI variation on the apparent temperature is strongly reduced for view zenith angles lower than 45°. In the nadir direction for example, the impact is not significant for LAI higher than 2, while it is maximum for this particular direction using the 1-D canopy representation. When LAI is 3 and the view zenith angle is 30°, LAI variations of +1 and

−1 induce apparent temperature variations of −0.21 K and +0.32 K for the 2-D representation and variations of −0.1 K and +0.15 K for the 3-D canopy representation. The differences induced by the canopy structure are explained by two main effects: (1) A saturation effect when LAI increases reduces the sensitivity of the canopy thermal emission to LAI variations. When the leaves are grouped within rows or crowns, the vegetation density is locally larger than if the same amount of leaves is homogeneously distributed within a vegetation layer. The saturation effect depends on the canopy structure and on the viewing direction. Generally speaking, a decrease of the canopy cover fraction implies a decrease of the LAI value for which saturation occurs. (2) The ground radiative contribution on the cover radiance is higher for heterogeneous canopies. When LAI increases, the ground emission contribution decreases whatever the canopy geometry. Moreover, the radiation emitted by the leaves and then scattered by the uncovered ground fraction increases for viewing directions close to the vertical.

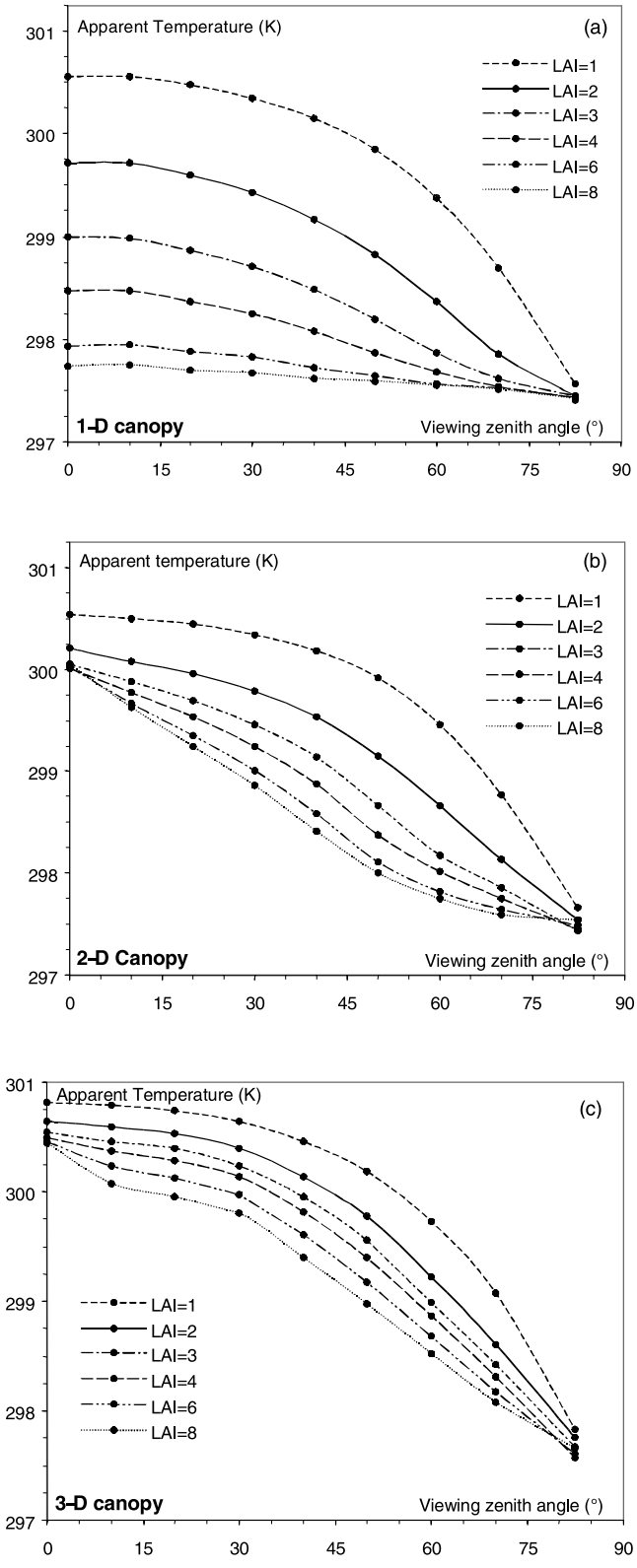

Figure 11. (opposite) Influence of variations in leaf are index (LAI) on the directional apparent temperature of three vegetation covers with (a) 1-D, (b) 2-D, and (c) 3-D canopy, respectively. The 1-D canopy is represented by superposed infinite layers of vegetation. The 2-D canopy consists of infinite rows of vegetation. We only plotted the apparent temperature obtained in the plane perpendicular to the rows. The 3-D canopy consists of trees randomly distributed over an infinite area. The LAI varies from 1 to 8. The temperature of the soil and leaves are 305 K and 298 K, respectively.

4.4.2. Cover Fraction

[55] The influence of cover fraction variations on the apparent temperature is illustrated in the case of a row plantation (Figure 12a). The cover fraction varies from 25% to 100%; these variations are obtained by modifying the distance between rows. The optical properties and temperature distributions within the cover are identical to the ones used in the previous section and LAI is 2. During the day, the soil temperature is higher than the vegetation temperature. As a consequence, the apparent temperature of the plantation increases when the cover fraction increases. In the nadir direction, a cover fraction variation of ±25% reduces or enhances the apparent temperature by 0.25 K. For view zenith angles higher than 30°, the radiance obtained for cover fractions equal to 75% and 100% are similar.

4.4.3. Leaf Angle Distribution

[56] Measurements carried out by *Guyot and Chasseray* [1981] on two wheat crops at the same physiological state showed that wheat having an erect growth pattern appeared systematically warmer than wheat having a spreading growth pattern. During the growing season, the authors observed differences between 1 K and 3 K on the apparent temperature in the vertical direction. The leaf angle distribution (LAD) describes the orientation of the leaves within the canopy. For various plant species, *Kimes and Kirchner* [1983b] measured significant daily variations of the LAD due to environmental factors such as sun position, wind speed or root zone water stress. The LAD cannot then be easily assessed from ground measurements. For this reason, most environmental studies assume a spherical angle distribution of the leaves [*Ross*, 1981]; that is, the normal vectors to the leaf surface are uniformly distributed in the 2π hemisphere. We evaluated the influence of the LAD in the simulated apparent temperature of a homogeneous cover and stressed errors that can be generated by using systematically a spherical leaf angle distribution. We made three simulations using different leaf angle distribution: planophil (highest probability to have horizontal leaves), spherical and

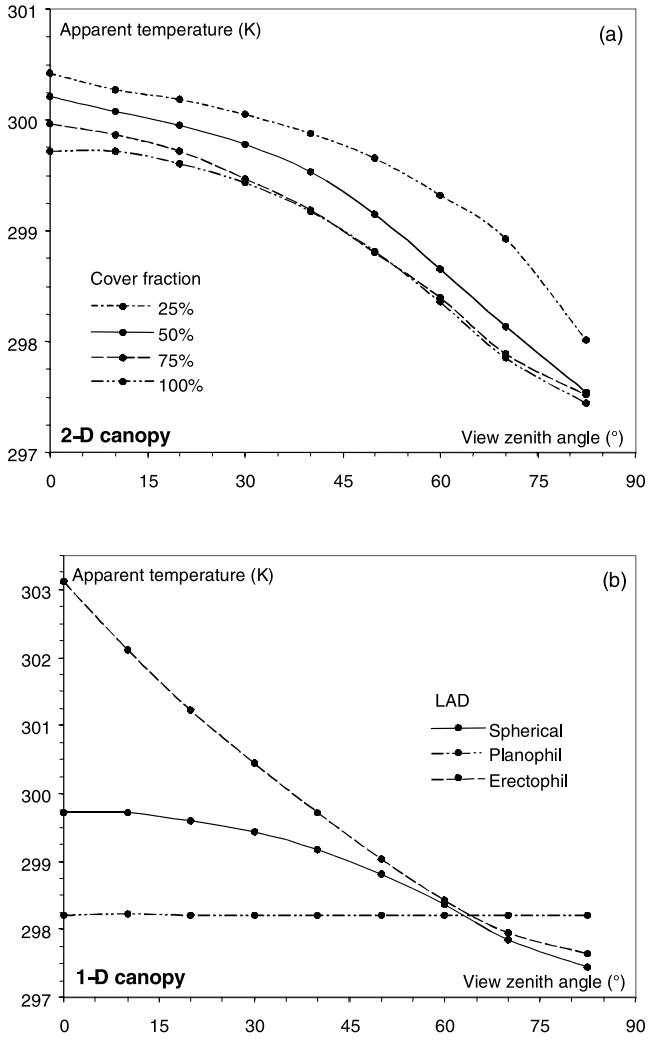

Figure 12. Relative impact of (a) the cover fraction and (b) the leaves orientation on the apparent temperature of a crop. (a) 2-D canopy representation with a cover fraction varying from 25% to 100%. (b) 1-D canopy representation with various leaf angle distribution (LAD) - spherical, planophil and erectophil. The LAI is 2. The temperature of the soil and leaves are 305 K and 298 K, respectively. The cover fraction is prescribed to 100%.

erectophil (highest probability to have vertical leaves). The differences obtained on the apparent temperature (Figure 12b) are maximum in the vertical direction, for which the canopy interception efficiency is maximum for a planophil distribution and minimum for an erectophil distribution. These differences depend on the temperature gradient between the soil and the vegetation. In comparison to results obtained with the spherical distribution, in the nadir direction, the cover appears 1.7 K cooler if the LAD is planophil (low soil radiative contribution) and 3.4 K warmer if the LAD is erectophil (high soil radiative contribution). The apparent temperature appears then to be more sensitive to variations in leaf angle distribution than to variations in cover fraction (see previous section). However, in reality, effects of both canopy geometry and leaves orientation are combined. This explain why numerous modeling studies [*Kimes et al.*, 1981; *Smith et al.*, 1981; *Prévot*, 1985; *McGuire et al.*, 1989] are based on accurate measurements of leaves orientation and position within the canopy.

5. Conclusion

[57] Thermal infrared remote sensing makes it possible to estimate continuously at various scales of space and time the temperature of terrestrial surfaces. The latter is an essential parameter to describe vegetation functioning and in particular water and energy budgets. Depending on surface characteristics and on acquisition configurations, radiometric measurements cannot be linked in a simple and direct way to surfaces temperatures.

[58] We presented a radiative transfer model that simulates the directional thermal infrared radiance of terrestrial surfaces. The model is an extension to the thermal infrared domain of the DART model, developed for the short wave domain. It simulates the radiative transfer within complex vegetation covers with a ray tracing approach combined with a discrete ordinate method. Its main originality is to take into account the three dimensional geometry of the cover. Consequently, it is a valuable tool to better understand and interpret remote sensing measurements. Using plausible optical properties of the cover components, we showed that within canopy scattering contributes to more than 1 K to the cover apparent temperature. To verify the analytical approach used to simulate radiative transfer, we first tested the model against a turbid-medium radiative transfer model in the case of homogeneous canopies. Then, a first validation was carried out over a cotton row crop using directional radiometric measurements. Finally, the sensitivity of the DART model to its major input parameters illustrated the influence of canopy structure on the directional apparent temperature of hypothetical tree covers and row plantations. The magnitude of the impact mainly depends on the temperature gradients within the cover, the canopy structure, and the viewing direction. For dense canopies, a neglect of canopy geometry can lead to underestimate the apparent temperatures by 1 K to 3 K. Similar variations were obtained in the case of homogeneous canopies with different leaf angle distributions.

[59] In the sensitivity studies, we used hypothetical or measured temperature distribution within the cover. Simulations stressed out the important role of the temperature distribution. The latter one is mainly driven by the canopy geometry and environmental factors (e.g., solar radiation, evapotranspiration and wind velocity). The extension of the DART model to the thermal infrared domain allows one to simulate the net radiation distribution. Our current efforts are dedicated to simulate the temperature distribution that satisfies local energy balance within the cover.

[60] **Acknowledgments.** The authors would like to thank J. Noilhan (CNRM, France) and B. Seguin (INRA, France) for their valuable comments.

References

Becker, F., F. Nerry, P. Ramanantsizehena, and M. Ph Stoll, Mesures d'émissivité angulaire par réflexion dans l'infrarouge thermique - Implications pour la télédétection, *Int. J. Remote Sens.*, *7*(12), 1751–1762, 1986.

Berger, X., A simple model for computing the spectral radiance of clear skies, *Solar Energy*, *40*(4), 321–333, 1988.

Boissard, L. K., G. Guyot, and R. D. Jackson, Factors affecting the radiative temperature of a vegetative canopy, *Application of Remote Sensing in Agriculture*, edited by M. D. Steven and J. A. Clark, Butterworths, London, 45–72, 1990.

Brutsaert, W., On a derivable formula for long wave radiation from clear skies, *Water Resour. Res.*, *11*, 742–744, 1975.

Caselles, V., J. A. Sobrino, and C. Coll, A physical model for interpreting the land surface temperature obtained by remote sensors over incomplete canopies, *Remote Sens. Environ.*, *39*, 203–211, 1992.

Chauki, H., A. Olioso, O. Taconet, C. Ottlé, and S. Outalha, Estimation de l'évaporation des couverts végétaux par inversion de modèles de télédétection, in *Physical Measurements and Signatures in Remote Sensing*, edited by Guyot and Phulpin, pp. 449–455, Malkema, Rotterdam, 1997.

Courault, D., B. Aloui, J. P. Lagouarde, P. Clastre, H. Nicolas, and C. Walter, Airborne thermal data for evaluating the spatial distribution of actual evapotranspiration over a watershed in oceanic climatic conditions—Application of semiempirical models, *Int. J. Remote Sens.*, *17*(12), 2281–2302, 1996.

Demarty, J., Développement et application du modèle SiSPAT-RS à l'échelle de la parcelle dans le cadre de l'expérience Alpilles ReSeDA, Ph.D. thesis, Univ. of Paris VII, 220 pp., 2001.

Elvidge, C. D., Thermal infrared reflectance of dry materials: 2.5–20.0 μm, *Remote Sens. Environ.*, *26*, 265–285, 1988.

François, C., C. Ottlé, and L. Prévot, Analytical parametrisation of canopy emissivity and directional radiance in the thermal infrared: Application on the retrieval of soil and foliage temperatures using two directional measurements, *Int. J. Remote Sens.*, *12*, 2587–2621, 1997.

Fuchs, M., Infrared measurement of canopy temperature and detection of plant water stress, *Theor. Appl. Climatol.*, *42*, 253–261, 1990.

Fuchs, M., E. T. Kanemasu, J. P. Kerr, and C. B. Tanner, Effect of viewing angle on canopy temperature measurements with infrared thermometers, *Agronomy Journal*, *59*(5), 494–496, 1967.

Gastellu-Etchegorry, J. P., V. Demarez, V. Pinel, and F. Zagolski, Modeling radiative transfer in heterogeneous 3-D vegetation canopies, *Remote Sens. Environ.*, *58*, 131–156, 1996.

Gastellu-Etchegorry, J. P., P. Guillevic, F. Zagolski, V. Demarez, V. Trichon, D. Deering, and M. Leroy, Modeling BRF and radiation regime of tropical and boreal forests, Part I, BRF, *Remote Sens. Environ.*, *68*, 281–316, 1999.

Guillevic, P., Modélisation des bilans radiatif et énergétique des couverts végétaux, Ph.D. Thesis, Paul Sabatier Univ., Toulouse, France, 181 pp., 1999.

Guyot, G., and E. Chasseray, Analyze de la signification physique et biologique de la température radiative d'un couvert végétal de céréales, in *Les colloques de l'INRA N°5*: "*Signatures spectrales d'objets en télédétection*," Avignon, France, 8–11 September 1981, pp. 379–389, 1981.

Hatfield, J. L., A. Perrier, and R. D. Jackson, Estimation of evapotranspiration at one time-of-day using remotely sensed surface temperatures, *Agricultural Water Management*, *7*, 341–350, 1983.

Huband, N. D. S., and J. L. Monteith, Radiative surface temperature and energy balance of a wheat canopy, I, Comparison of radiative and aerodynamic canopy temperature, *Bound.-Layer Meteorol.*, *36*, 1–17, 1986.

Huete, A. R., R. D. Jackson, and D. F. Post, Spectral response of plants canopy with different soil backgrounds, *Remote Sens. Environ.*, *15*, 37–53, 1985.

Inoue, Y., B. A. Kimball, R. D. Jackson, P. J. Pinter Jr., and R. J. Reginato, Remote estimation of leaf transpiration rate and stomatal resistance based on infrared thermometry, *Agric. For. Meteorol.*, *51*, 21–33, 1990.

Jackson, R. D., R. J. Reginati, and S. B. Idso, Wheat canopy temperature: A practical tool for evaluating water requirements, *Water Resour. Res.*, *13*, 651–662, 1977.

Jackson, R. D., R. J. Reginato, P. J. Pinter, and S. B. Idso, Plant canopy information extraction from composite scene reflectance of row crops, *Appl. Opt.*, *18*, 3775–3782, 1979.

Kimes, D. S., Effects of vegetation canopy structure on remotely sensed canopy temperature, *Remote Sens. Environ.*, *10*, 165–174, 1980.

Kimes, D. S., and J. A. Kirchner, Directional radiometric measurements of row-crop temperatures, *Int. J. Remote Sens.*, *4*(2), 299–311, 1983a.

Kimes, D. S., and J. A. Kirchner, Diurnal variation of vegetation canopy structure, *Int. J. Remote Sens.*, *4*(2), 257–271, 1983b.

Kimes, D. S., S. B. Idso, P. J. Pinter, R. D. Jackson, and R. J. Reginato, Complexities of nadir-looking radiometric temperature measurements of plant canopies, *Appl. Opt.*, *19*, 2162–2168, 1980.

Kimes, D. S., J. A. Smith, and L. E. Link, Thermal IR exitance model of a plant canopy, *Appl. Opt.*, *20*, 623–632, 1981.

Labed, J., and M. P. Stoll, Angular variation of land surface spectral emissivity in the thermal infrared: Laboratory investigations on bare soils, *Int. J. Remote Sens.*, *12*(11), 2299–2310, 1991.

Lagouarde, J. P., Y. Kerr, and Y. Brunet, An experimental study of angular effects on surface temperature for various plant canopies and bare soil, *Agric. For. Meteorol.*, *77*, 167–190, 1995.

Lagouarde, J. P., E. Pradel, and C. Sanz, Estimation des flux de surface à l'échelle régionale, *Actes de l'Ecole-Chercheurs INRA en Bioclimatologie*, 25–29 March 1996, vol. 2, pp. 361–382, Le Croisic, France, 1996.

Luquet, D., Suivi de l'état hydrique des plante par infrarouge thermique: Analyze expérimentale et modélisation 3D de la variabilité thermique au sein d'une culture en rang de cotonnier, Ph.D. Thesis, Institut National Agronomique Paris Grignon, Paris, France, 164 pp., 2002.

Luquet, D., J. Dauzat, A. Vidal, P. Clouvel, and A. Bégué, 3D simulation of leaves temperature in a cotton-row crop: toward an improvement of thermal infrared signal interpretation to monitor crop water status, in *8th International Symposium Physical Measurements & Signatures in Remote Sensing* (ISPRS, ed.), pp. 493–499, Aussois, France, 2001.

McGuire, M. J., L. K. Balik, J. A. Smith, and B. A. Hutchison, Modeling directional radiance from a forest canopy, *Remote Sens. Environ.*, *27*, 169–186, 1989.

Norman, J. M., and J. M. Welles, Radiative transfer in an array of canopies, *Agronomy J.*, *75*, 481–488, 1983.

Norman, J. M., M. C. Anderson, G. R. Diak, J. Mecikalski, and W. P. Kustas, Regional estimates of surface fluxes using temperature differences from GOES thermal images, *Proceedings of the 7th International Symposium on Physical Measurements and signatures in Remote Sensing*, April 1997, Courchevel, France, edited by G. Guyot and T. Phulpin, pp. 449–455, Balkema (Rotterdam, The Netherlands), pp. 401–411, 1997.

Olioso, A., Simulating the relationship between thermal emissivity and the normalized difference vegetation index, *Int. J. Remote Sens.*, *16*, 3211–3216, 1995.

Olioso, A., H. Chauki, D. Courault, and J.-P. Wigneron, "Estimation of evapotranspiration and photosynthesis by assimilation of remote sensing data into SVAT models", *Remote Sens. Environ.*, *68*, 341–356, 1999.

Ottlé, C., and D. Vidal-Madjar, Assimilation of soil moisture inferred from infrared remote sensing in a hydrological model over the HAPEX-MOBILHY region, *J. Hydrol.*, *158*, 241–264, 1994.

Paw, K. T., Development of models for thermal infrared radiation above and within plant canopies, *ISPRS J. Photogrammetry Remote Sens.*, *47*, 189–203, 1992.

Prévot, L., Modélisation des échanges radiatifs au sein des couverts végétaux - Application à la télédétection - Validation sur un couvert de mäs, Ph.D. Thesis, Univ. of Paris VI, 135 pp., 1985.

Ross, J., The radiation regime and architecture of plant stands, W. Junk, The Hague, the Netherlands, 391 pp., 1981.

Sabins, F. F., Remote sensing—Principles and interpretation, 2nd edition, W. H. Freeman, New York, 449 pp., 1987.

Salisbury, J. W., and D. M. D'Aria, Emissivity of terrestrial materials in the 8–14 μm atmospheric window, *Remote Sens. Environ.*, *42*, 83–106, 1992.

Seguin, B., and B. Itier, Using midday surface temperature to estimate daily evaporation from satellite thermal IR data, *Int. J. Remote Sens.*, *4*, 371–383, 1983.

Seguin, B., J. P. Lagouarde, and M. Savane, The assessment of regional crop water conditions from meteorological satellite thermal infrared data, *Remote Sens. Environ.*, *35*, 141–148, 1991.

Smith, J. A., K. J. Ranson, D. Nguyen, L. Balick, L. E. Link, L. Fritschen, and B. Hutchison, Thermal vegetation canopy model studies, *Remote Sens. Environ.*, *11*, 311–326, 1981.

Sobrino, J. A., and V. Caselles, Thermal infrared radiance model for interpreting the directional radiometric temperature of a vegetative surface, *Remote Sens. Environ.*, *33*, 193–199, 1990.

Stewart, J. B., W. P. Kustas, K. S. Humes, W. D. Nichols, M. S. Moran, and H. A. R. de Bruin, Sensible heat flux - Radiometric surface temperature relationship for 8 semi-arid areas, in *Proceedings of Workshop on "Thermal remote sensing of the energy and water balance over vegetation in conjunction with other sensors*," La Londe les Maures, France, September 1993, CEMAGREF ed., pp. 27–30, 1993.

Sutherland, R. A., and J. F. Bartholic, Significance of Vegetation in Interpreting Thermal Radiation from a Terrestrial Surface, *J. Appl. Meteorol.*, *16*(8), 759–763, 1977.

Taconet, O., R. Bernard, and D. Vidal-Madjar, Evapotranspiration over an agricultural region using a surface flux/temperature model based on NOAA/AVHRR data, *J. Climate Appl. Meteorol.*, *25*, 284–307, 1986.

Taconet, O., A. Olioso, M. Ben Mehrez, and N. Brisson, Seasonal estimation of evaporation and stomatal conductance over a soybean field using surface infrared temperature, *Agric. For. Meteorol.*, *73*, 321–337, 1995.

J. Demarty and L. Prévot, INRA Avignon - Unité CSE, Domaine Saint Paul, site Agroparc, 84914 Avignon Cedex 9, France. (jdemarty@avignon.inra.fr; lprevot@avignon.inra.fr)

J. P. Gastellu-Etchegorry, Centre d'Études Spatiales de la BIOsphère, 18 avenue Édouard Belin, bpi 2801, 31401 Toulouse Cedex 4, France. (Jean-Philippe.Gastellu@cesbio.cnes.fr)

P. Guillevic, Hydrologie des Milieux Urbains/Division Eau, Laboratoire Central des Ponts et Chaussées (LCPC), Route de Bouaye, BP 4129, 44341 Bouguenais Cedex, France. (pierre.guillevic@lcpc.fr)